Journal of Nanophotonics

SPIEDigitalLibrary.org/jnp

# Characterization of all-normal-dispersion microstructured optical fiber via numerical simulation of passive nonlinear pulse reshaping and single-pulse flat-top supercontinuum

Oleksiy V. Shulika
Igor A. Sukhoivanov
Gabriel Ramos-Ortiz
Igor V. Guryev
Sergii O. Iakushev
José Amparo Andrade Lucio

SPIE

# Characterization of all-normal-dispersion microstructured optical fiber via numerical simulation of passive nonlinear pulse reshaping and single-pulse flat-top supercontinuum

**Oleksiy V. Shulika,[a] Igor A. Sukhoivanov,[a,*] Gabriel Ramos-Ortiz,[b] Igor V. Guryev,[a] Sergii O. Iakushev,[c] and José Amparo Andrade Lucio[a]**

[a]Universidad de Guanajuato, Division de Ingenerías Campus Irapuato-Salamanca, Salamanca, Guanajuato 36885, Mexico

[b]Centro de Investigaciónes en Óptica, León, Guanajuato 37150, México

[c]Kharkov National University of Radio Electronics, R&D Laboratory "Photonics," Kharkov 61166, Ukraine

**Abstract.** The supercontinuum (SC) generated by pumping in anomalous dispersion is sensitive to the input pulse fluctuations and pump laser's shot noises and does not possess a single-pulse waveform, so the incident pulse becomes a noise-like train of spikes. A simple method of creating pulsed lasers with either pulse-maintaining ultrabroad SC or specially shaped pulse waveforms can be implemented using all-normal-dispersion microstructured optical fibers (ANDi-MOFs). An ANDi-MOF with a simple topology and dispersion profile maximum at 800 nm was designed using the effective index method. Its properties and suitability were characterized via numerical simulation of femtosecond parabolic pulse formation and generation of an octave-spanning pulse-maintaining SC using a generalized propagation equation. The designed ANDi-MOF is suitable for resolving both problems and allows some detuning of the pulse's wavelength around 800 nm. However, a better choice for SC generation is pumping at or near the wavelength where the third-order dispersion becomes zero. This configuration benefits from the absence of pulse break-up under large pulse energies, which appears otherwise. The fiber can provide a low-cost method for developing supercontinuum sources and a solution to the problems of parabolic waveform formation to meet the needs of optical signal processing and pulse amplification and compression.
*© The Authors. Published by SPIE under a Creative Commons Attribution 3.0 Unported License. Distribution or reproduction of this work in whole or in part requires full attribution of the original publication, including its DOI.* [DOI: 10.1117/1.JNP.8.083890]

**Keywords:** photonic crystal fibers; microstructured optical fibers; pulse-maintaining supercontinuum; passive nonlinear pulse reshaping; all-normal-dispersion microstructured optical fibers; all-normal-dispersion photonic crystal fibers.

Paper 13088SSP received Oct. 15, 2013; revised manuscript received Jan. 27, 2014; accepted for publication Jan. 28, 2014; published online Feb. 27, 2014.

## 1 Introduction

Ultrabroad spreading of ultrashort pulses propagating in an optical fiber involves a variety of nonlinear phenomena. The bandwidth of the spreading can reach several octaves and is called a supercontinuum (SC). Great interest in this field was inspired by the invention of microstructured optical fibers (MOFs), which have allowed SC generation for a much wider range of source parameters than was possible with bulk media or conventional fibers. Despite the great potential of MOFs for controlling the dispersive and nonlinear properties of the guiding medium, most research has concentrated on pumping in the anomalous dispersion region.[1] These studies have uncovered the key contributions of soliton fission and modulation instability to SC generation under pumping in the anomalous dispersion regime. In turn, these results have allowed the

*Address all correspondence to: Igor A. Sukhoivanov, E-mail: i.sukhoivanov@ieee.org

invention of other methods of SC generation such as CW pumping and pumping with nano/picosecond pulses.[1] Since a SC can be generated with virtually any laser source and any optical fiber, one may give the impression that this line of research has already exhausted itself. This is not the case.

The broadening mechanism of the SC generated in anomalous dispersion is dominated by the soliton dynamics and soliton fission, which are sensitive to the input pulse fluctuations and pump laser's shot noise. Another drawback of this type of SC is the lack of coherence and the fact that in the time domain, it does not exhibit a single-pulse waveform but has the form of a noise-like train of spikes. However, pumping in the normal dispersion region of optical fibers could benefit from the generation of octave-spanning supercontinua, which are characterized by the preservation of a single-pulse waveform in the time domain and perfect temporal coherence and spectral properties[2–4] suitable for efficient external recompression. This is important because of the practical demands of few-cycle laser pulses in time-resolved studies of fundamental processes in physics, chemistry, and biology. Although these applications drive the development of various techniques for generating few-cycle pulses, the generation of high-quality few-cycle pulses by inexpensive and simple methods is still challenging.

Passive nonlinear pulse reshaping is another type of nonlinear phenomenon that occurs in the normal dispersion regime. It provides a simple option for the transformation of pulse waveforms needed for many practical applications. Flat-top (rectangular-like), triangular, and parabolic pulses are used in all-optical signal processing, ultrahigh-speed optical systems, and nonlinear optics.[5] In particular, the interest in parabolic pulses in recent years was inspired by their unique properties.[6] These pulses propagate self-similarly in an active fiber in the presence of normal dispersion and nonlinearity; therefore, they are called "similaritons." The amplitude and width scaling in this case depend only on the amplifier parameters and input pulse energy. Parabolic pulses have found numerous applications in pulse amplification and compression[7] as well as in optical communications.[5,7] These include optical regeneration,[8] pulse re-timing,[9] the optimization of return-to-zero optical receivers,[10] and mitigation of linear waveform distortions.[11]

Conventional single-mode fibers provide only a limited range of normal dispersion. Further, even if the pump wavelength is within the normal dispersion range, the huge broadening of the incident pulse will cause part of the pulse spectrum to appear in the anomalous dispersion range. An alternative to conventional single-mode fibers is microstructured ones, which provide much more freedom for engineering the dispersion profile and nonlinearity than their conventional counterparts. The novelty of this paper lies in its presentation of an MOF with a simple topology, which possesses normal dispersion spanning more than one octave around 800 nm and is suitable for passive nonlinear pulse reshaping on a femtosecond timescale and the production of a single-pulse flat-top SC spanning almost two octaves.

## 2 Fiber Design

The all-normal-dispersion MOF (ANDi-MOF) was designed so that it provides an extremum of the all-normal-dispersion profile at exactly 800 nm. This prerequisite is considered in the context of the femtosecond duration of the incident pulses: Ti:Sapphire femtosecond oscillators generating nominally at 800 nm are the most widespread ones to date. However, other wavelengths can be targeted, as the microstructured topology of MOFs allows great freedom in dispersion design via manipulation of the waveguide dispersion. Silica glass is chosen as the material of the ANDi-MOF under design because of its perfect optical characteristics around the target wavelength. It will also maintain the technological compatibility of this fiber with conventional single-mode fibers and devices made of them. The topology of the fiber cross-section should be as simple as possible to facilitate fabrication of the ANDi-MOF using existing methods. Therefore, as a starting point for design, we chose a solid-core MOF with microstructured cladding made of air holes in a triangular lattice configuration. The cross-sectional topology does not contain any nanosize inclusions or extreme topological elements such as suspended nanosize cores. Thus, the cross-section that we used benefits from its simplicity and well-developed fabrication methods such as the stack-and-draw technique. The configuration of the fiber cross-section is also attractive from a theoretical viewpoint because it allows parameterization within the classical fiber

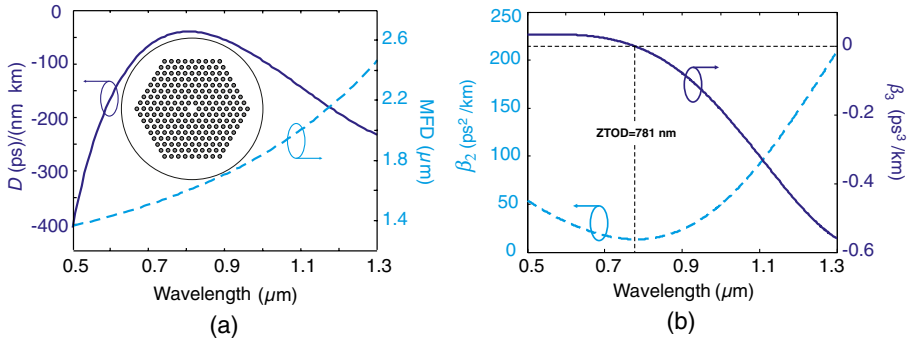


**Fig. 1** (a) Calculated dispersion profile and mode field diameter of ANDi-MOF. (b) Corresponding spectral dependencies of second- and third-order dispersion coefficients.

theory, providing a fast parameter sweep for design purposes. However, the microstructured cladding should be thick enough, so that parameterization would be possible. On the other hand, the sufficiently large thickness of the microstructured cladding reduces the confinement losses in MOFs. However, the cladding should not be too thick from the viewpoint of fabrication. Thus, there is a trade-off, which is reached when the number of rings is seven or eight.

The dispersion profile and mode field diameter of the ANDi-MOF were found semi-analytically[12] with a prior cross-check by the finite element method. Figure 1 shows the dispersion profile of the designed fiber in terms of the dispersion parameter $D$ and the second-order dispersion coefficient. The topological parameters of the cross-section, which provide the dispersion properties in Fig. 1, are the pitch, $\Lambda = 1\ \mu$m, and the relative hole diameter, $d/\Lambda = 0.5$. We will see below that the position of the pulse wavelength relative to the zero-third-order dispersion (ZTOD) wavelength is important for the development of SC in the ANDi-MOF. Thus, Fig. 1 also shows the third-order dispersion coefficient and demonstrates that the ZTOD wavelength is 781 nm for the fiber considered here. The curves in Fig. 1 are the input data for the numerical characterization of the ANDi-MOF's suitability for passive nonlinear reshaping at a femtosecond timescale and the generation of pulse-maintaining SC.

## 3 Pulse Propagation Model

### 3.1 *Passive Nonlinear Pulse Reshaping at Femtosecond Time Scale*

Picosecond pulses are known to be described well by the nonlinear Schrödinger equation. However, as the pulse duration decreases to the femtosecond range, the higher-order nonlinear effects have to be included, namely pulse self-steepening and intrapulse Raman scattering. In this case, the pulse propagation equation is frequently referred to as the generalized nonlinear Schrödinger equation (GNLSE). It is formulated in terms of the electric field envelope, $A = A(z, T)$, in a retarded reference time frame, $T = t - \beta_1 z$, like its simplified counterpart and has the form

$$\frac{\partial A}{\partial z} = -\frac{\alpha}{2}A - \left(\sum_{n\geq 2}\beta_n \frac{i^{n-1}}{n!}\frac{\partial^n}{\partial T^n}\right)A + i\gamma\left(1 + \frac{1}{\omega_0}\frac{\partial}{\partial T}\right) \times \left[(1 - f_R)A|A|^2 + f_R A\int_0^\infty h_R(\tau)|A(z, T-\tau)|^2 \mathrm{d}\tau\right], \quad (1)$$

where $\alpha$ is the attenuation constant, $\gamma$ is the nonlinear coefficient, and $\beta_n$ is the dispersion coefficient obtained by a Taylor series expansion of the propagation constant $\beta(\omega)$ around the pulse center frequency $\omega_0$.

The pulse center frequency corresponds to a wavelength of 800 nm in our study. The response function, $R(t) = (1 - f_R)\delta(t) + f_R h_R(t)$, includes both the instantaneous electronic and delayed Raman contributions with $f_R = 0.18$, representing the fractional contribution of the delayed Raman response. For the Raman response function of the silica fiber, $h_R(t)$, the analytical expression is used[13]

$$h_R(t) = \frac{\tau_1^2 + \tau_2^2}{\tau_1 \tau_2} \exp\left(-\frac{t}{\tau_2}\right) \sin\left(\frac{t}{\tau_1}\right), \tag{2}$$

where $\tau_1 = 12.2$ fs and $\tau_2 = 32$ fs.

In the general case, a pulse launched into the fiber can be chirped, i.e., have time-dependent instantaneous frequency. We include chirping in the initial pulse as follows:

$$A_{\text{chirp}} = A_{\text{unchirp}} \exp\left(iC\frac{T^2}{2T_0^2}\right), \tag{3}$$

where $A_{\text{unchirp}}$ is the waveform of an unchirped initial pulse, $C$ is the chirp parameter, and $T_0$ is the initial pulse duration (half-width at the $1/e$-intensity level), which is nominally 100 fs in this article. Equation (3) describes the linear dependence of the instantaneous frequency $\omega = \omega_0 + CT/T_0^2$ (linear chirping).

### 3.2 *Criteria for Parabolicity*

The pulse quality is estimated using the deviation of its temporal/spectral intensity profile, $|A(T)|^2$, and a parabolic fit, $|A_{\text{p}}(T)|^2$, of the same energy, which is expressed as the misfit parameter $M$[14]

$$M^2 = \frac{\int (|A|^2 - |A_{\text{p}}|^2)^2 \mathrm{d}\tau}{\int |A|^4 \mathrm{d}\tau}. \tag{4}$$

The expression for a parabolic pulse of energy $U_{\text{p}} = 4P_{\text{p}}T_{\text{p}}/3\sqrt{2}$ is given by[15–17]

$$A_{\text{p}}(T) = \begin{cases} \sqrt{P_{\text{p}}}\sqrt{1 - 2T^2/T_{\text{p}}^2}, & |T| \le T_{\text{p}}/\sqrt{2} \\ 0, & |T| > T_{\text{p}}/\sqrt{2} \end{cases}, \tag{5}$$

where $P_{\text{p}}$ is the peak power of the parabolic pulse, $T_{\text{p}}$ is the duration of the parabolic pulse [(full-width at half-maximum (FWHM)], and $A_{\text{p}}$ is the pulse magnitude.

The misfit parameter $M$ allows the estimation of the pulse shape imperfection with respect to a parabolic shape; smaller values of $M$ indicate a better fit to the parabolic waveform. One can consider a pulse shape to be close enough to the parabolic one when $M < 0.04$.

### 3.3 *Single-Pulse SC*

A single-pulse SC (SPSC) is simulated using the GNLSE [Eq. (1)]. The fiber loss is neglected because short pieces of the fiber are considered. The dispersion parameters of the designed ANDi-MOF are taken up to the eighth order because of the broad spreading of the pulse. For 800 nm, they are $\beta_2 = 1.363 \times 10^1$ ps$^2$/km, $\beta_3 = -8.65 \times 10^{-3}$ ps$^3$/km, $\beta_4 = 1.674 \times 10^{-4}$ ps$^4$/km, $\beta_5 = -5.48 \times 10^{-7}$ ps$^5$/km, $\beta_6 = 1.59 \times 10^{-9}$ ps$^6$/km, $\beta_7 = -3.801 \times 10^{-12}$ ps$^7$/km, and $\beta_8 = 4.0 \times 10^{-15}$ ps$^8$/km. The calculated nonlinear parameter at 800 nm is $\gamma = 113.31/$ (W · km).

## 4 Results and Discussion

### 4.1 *Femtosecond Parabolic Pulses*

The unique properties of ANDi-MOFs are very attractive for nonlinear pulse reshaping. Even very short pulses with a large spectral bandwidth can be reshaped, because the normal dispersion spans the entire spectral range. The relatively flat-top dispersion profile of the ANDi-MOF is highly beneficial for pumping, because, in this case, the impact of higher-order dispersion on the reshaping process is reduced, which is also important for very short pulses. The dispersion profile of an ANDi-MOF can be tuned and provides desired flat-top region in a wide spectral band from the visible to the near-infrared.

Figure 2 shows the dependence of the misfit parameter $M$ on the energy of the incident pulse and fiber length $z$ for the ANDi-MOF presented above. The incident pulse has a Gaussian shape in Figs. 2(a) and 2(b) and a hyperbolic secant shape in Figs. 2(c) and 2(d). The filled areas show the array of parameters providing the formation of high-quality parabolic pulses with $M < 4\%$, in which we are interested. The dashed lines yield pairs of parameters (incident pulse energy—fiber length) that produce formation of parabolic pulses with a certain duration (FWHM), shown on each line as a femtosecond value. Thus, the places where the lines of constant duration cross the filled areas yield ranges of pulse energies and fiber lengths that will produce femtosecond parabolic pulses. Two cases are combined in the same figure: pulse reshaping at short propagation distances (approach A), as shown in Figs. 2(a) and 2(c), and in the steady-state propagation regime (approach B),[17] as shown in Figs. 2(b) and 2(d). Because the fiber has been designed with a sufficiently large nonlinear parameter, parabolic pulses can be obtained using pulses with a rather small energy; the picojoule range (9 to 80 pJ) is sufficient. Thus, the designed ANDi-MOF can be used for nonlinear reshaping with gigahertz femtosecond lasers, which usually generate picojoule pulses,[18,19] or under conditions of low-quality coupling when a large part of the incident pulse is scattered. Another important feature is that the designed fiber provides a small amount of normal dispersion ($\beta_2$). Therefore, the dispersion length is large for a given pulse duration. Practically, this allows the use of shorter initial pulses, while maintaining a fiber length that is long for easy operation.

Another interesting feature is the expanding of the filled area toward larger energies for the case of a chirped Gaussian incident pulse reshaped in the steady-state propagation regime [Fig. 2(b)]. It means that one uses a larger range of pulse energies and fiber lengths when applying chirped incident pulses. However, the price of this freedom is an increase in the output pulse duration, which can ultimately enter the subpicosecond or picosecond range. The hyperbolic secant pulses are not as useful because of the narrow filled areas in Figs. 2(c) and 2(d).

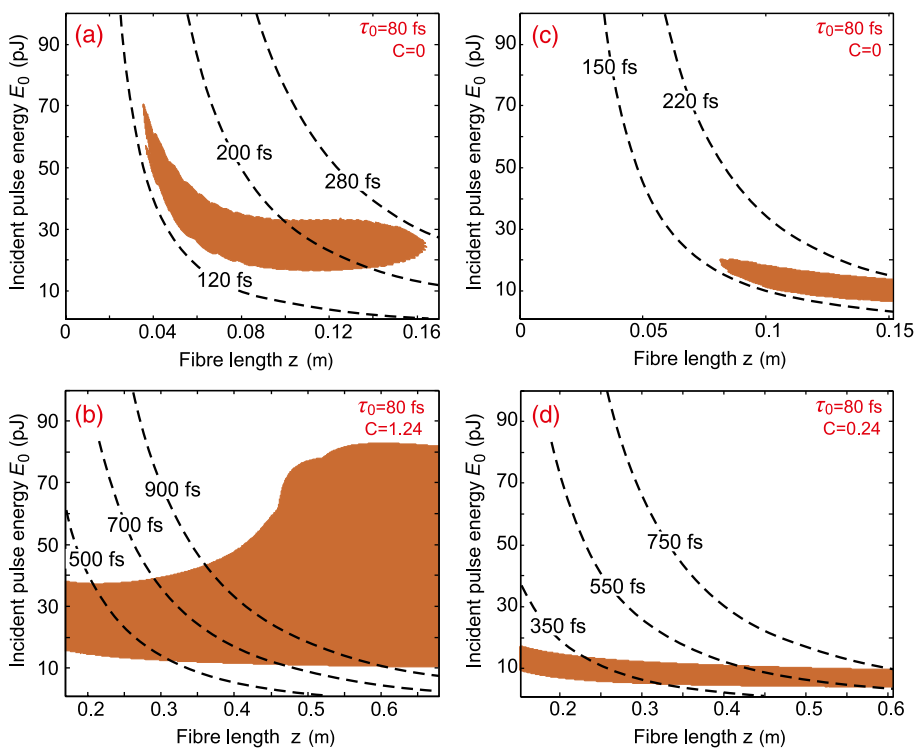


**Fig. 2** Misfit parameter maps, $M(E_0, \tau)$, and contour curves of pulse duration, $\tau(E_0, z)$ (dashed lines). The femtosecond values on the dashed black lines show the duration [full width at half maximum (FWHM)] of parabolic pulses at fiber output. Top row (a and c) shows the results for $z \leq L_D$, and bottom row (b and d) shows those for $L_D < z < 4L_D$. Left column (a and b) shows the results for incident Gaussian pulse, and right column (c and d) shows those for incident secant hyperbolic pulse. Insets in upper right corners show the FWHM and chirp of incident pulse.

From the misfit parameter maps of $M(E_0, z)$ and the contour curves of the pulse duration $\tau(E_0, z)$, presented in Fig. 2, one can find the shortest parabolic pulses available for the given fiber and initial pulse parameters. In particular, for a given map of the misfit parameter, $M(E_0, z)$, operation at a lower pulse energy (the bottom of the filled area) is preferable because the parabolic pulse duration is shorter here for a given fiber length.

Keeping in mind the last observation, we calculated two examples of parabolic pulses obtained from the misfit parameter maps presented in Figs. 2(a) and 2(b). Figure 3 shows the characteristics of these parabolic pulses, which were obtained from 80-fs Gaussian pulses in the short propagation distance and steady-state propagation regimes, approaches A and B, respectively. One can see that both parabolic pulses [Figs. 3(a) and 3(d)] are indeed very close to the ideal parabolic fit profile, and at the short propagation distance (10 cm), the pulse width (FWHM) is 156 fs. In the steady-state regime (30 cm), it is larger (466 fs); the reason is obviously that the longer propagation distance is required for the appearance of the steady-state regime. However, the longer propagation distance provides more linear chirp over the entire pulse width [compare Figs. 3(b) and 3(e)], which is preferable for efficient pulse compression. In the steady-state propagation regime, the obtained spectrum is also

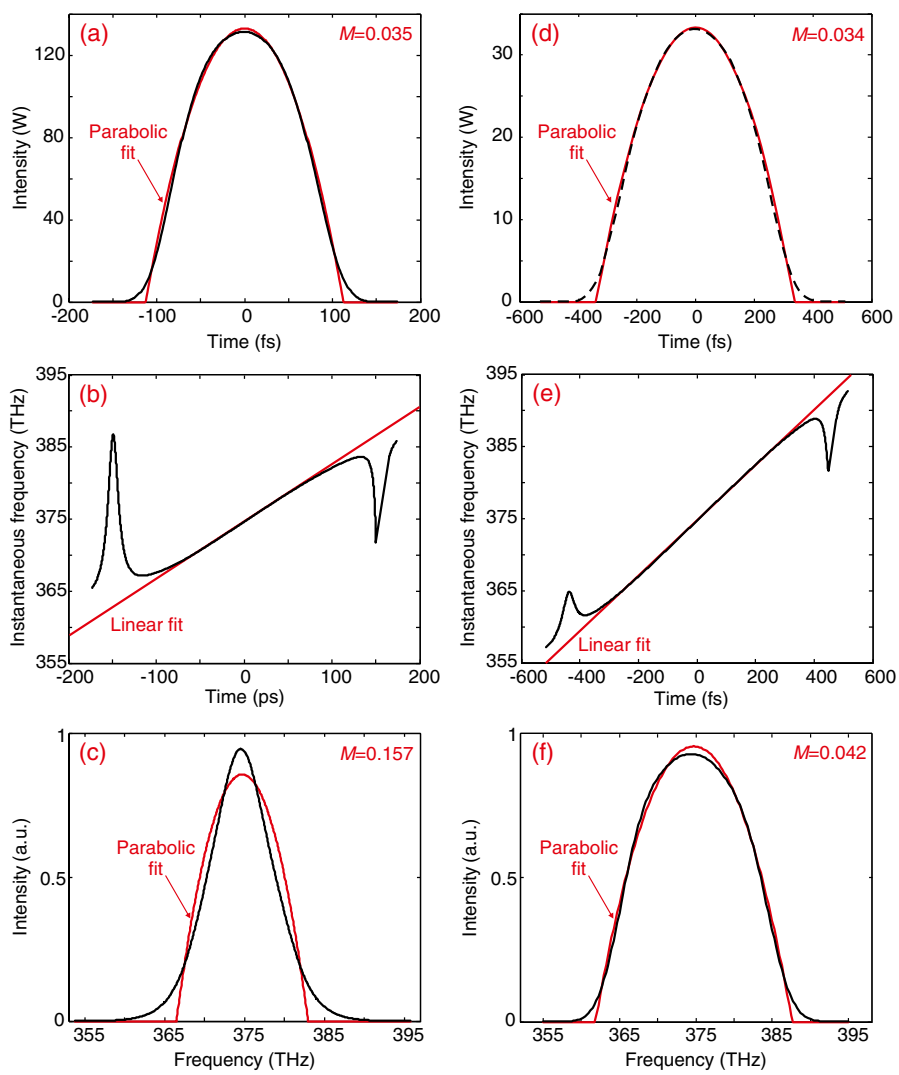


**Fig. 3** Parabolic pulses generated in ANDi-MOF. Left column (a, b, and c) shows the results (temporal intensity, chirp, spectrum) of parabolic pulses obtained from initial unchirped Gaussian pulse ($\tau_0 = 80$ fs, $E_0 = 20$ pJ) at fiber length of 10 cm. Right column (d, e, and f) shows the result of parabolic pulse obtained in the steady-state propagation regime from initial chirped Gaussian pulse ($\tau_0 = 80$ fs, $E_0 = 15$ pJ, $C = 1.24$) at fiber length of 30 cm.

very close to the ideal parabolic profile [Fig. 3(f)], whereas at the short propagation distance, the spectral profile differs greatly from the parabolic one [Fig. 3(c)] and resembles a Gaussian curve. Referring to Fig. 2(b), one can see that a shorter fiber (e.g., 20 cm) can be used in the steady-state regime to obtain shorter parabolic pulses; however, in this case, the spectra of the output pulses will deviate more from the parabolic profile.

Thus, the main advantage of approach A is the formation of very short parabolic pulses with broadening by a factor of ~2. The minimal width of the parabolic pulses in this case is generally limited by the duration of the incident pulses. However, a very short fiber (a few centimeters) is also required to obtain the shortest parabolic pulses. In this case, it is reasonable to use fibers with less second-order dispersion, which allows the use of shorter initial pulses while maintaining a fiber length that is sufficient to maintain usability. Unchirped Gaussian pulses are preferable for the problem described.

In the steady-state propagation regime,[14] approach B, one obtains longer parabolic pulses with a broadening factor of ~5 to 6. The advantage of this case is the asymptotic properties of the output pulses; i.e., they can be considered as quasi-similaritons. Further, this is a huge benefit for pulse postprocessing. Working within approach B requires that the incident pulse be chirped and the fiber length is usually >10 cm.

### 4.2 *Single-Pulse SC*

Previously, we considered the possibility of generation of an SPSC in the ANDi-MOF presented above under the incidence of an 80-MHz train of 100-fs unchirped Gaussian pulses at 800 nm.[20] We found that a wide SPSC spanning from the violet to the near-infrared can be obtained. However, under experimental conditions, the pulse wavelength $\lambda_p$ can be influenced by various factors and differs somewhat from the nominal wavelength. Therefore, in this section, we present the results of an SPSC simulation under variable pulse wavelengths and energies. The results can be interpreted as either a demonstration of the robustness of the ANDi-MOF presented or a search for the conditions for generating the optimal SPSC.

Figure 4 shows the simulated spectra (right column) and pulse waveforms (left column) at the output of the ANDi-MOF designed under the incidence of pulses from 5 to 65 nJ and three different pulse wavelengths near 800 nm. The results presented are for a 10-cm-long fiber. At this length, there are no notable variations in the spectral content, and the spectrum has its final shape. The damage threshold of commercial MOFs is a peak power of about 200 kW, depending on many factors. This value corresponds to about 20 nJ pulses with a duration of 100 fs, which we used in the calculations. Thus, some of the SPSCs in the figure reflect a type of unphysical cases; we show them for comparison. When pumped at 800 nm, the SC spectrum is quite flat for a 5-nJ pump with the exception of a small dip at the pump wavelength, which becomes stronger for a 10-nJ pump. Increasing the pulse energy results in the appearance of optical-shock-type signatures, which are clearly visible at 16 nJ and become apparent in an oscillatory structure in the pulse temporal profile and in the spectrum. The oscillations arise only at the trailing edge of the pulse and on the short-wavelength side of the spectrum. Further analysis of Fig. 4 with shifted pulse wavelengths ($\lambda_p = 800\ \text{nm} \pm 10\ \text{nm}$) suggests that optical shock can be avoided by blue shifting $\lambda_p$. Contrariwise, the optical shock appears earlier if the pulse wavelength $\lambda_p$ is shifted to the long-wavelength side. In terms of the type of threshold energy for shock formation, 790-nm pumping possesses the largest threshold: more than 65 nJ. In contrast, 810-nm pumping has the lowest threshold energy among the results presented: ~10 nJ. Further, 800-nm pumping has an intermediate value of ~16 nJ. Observing that pulses with a larger energy produce an SPSC with a larger bandwidth, we arrive at the self-evident conclusion that to obtain the largest bandwidth possible for a given ANDi-MOF without shock-like oscillations, it should be pumped on the blue side from the maximum of the dispersion curve. Optical shock formation is usually believed to be a consequence of self-steepening in the presence of normal group velocity dispersion.[21] However, the variation in the dispersion of the ANDi-MOF presented here is rather small within the range of pulse wavelengths considered here; i.e., all three cases of pumping considered here possess the same value of the dispersion parameter $D \approx -40.1\ \text{ps}\,(\text{nm} \cdot \text{km})$, corresponding to $\beta_2 = 13.63\ \text{ps}^2/\text{km}$. In this case, we would not observe optical shock signatures when pumping with pulses of the same energy but at different

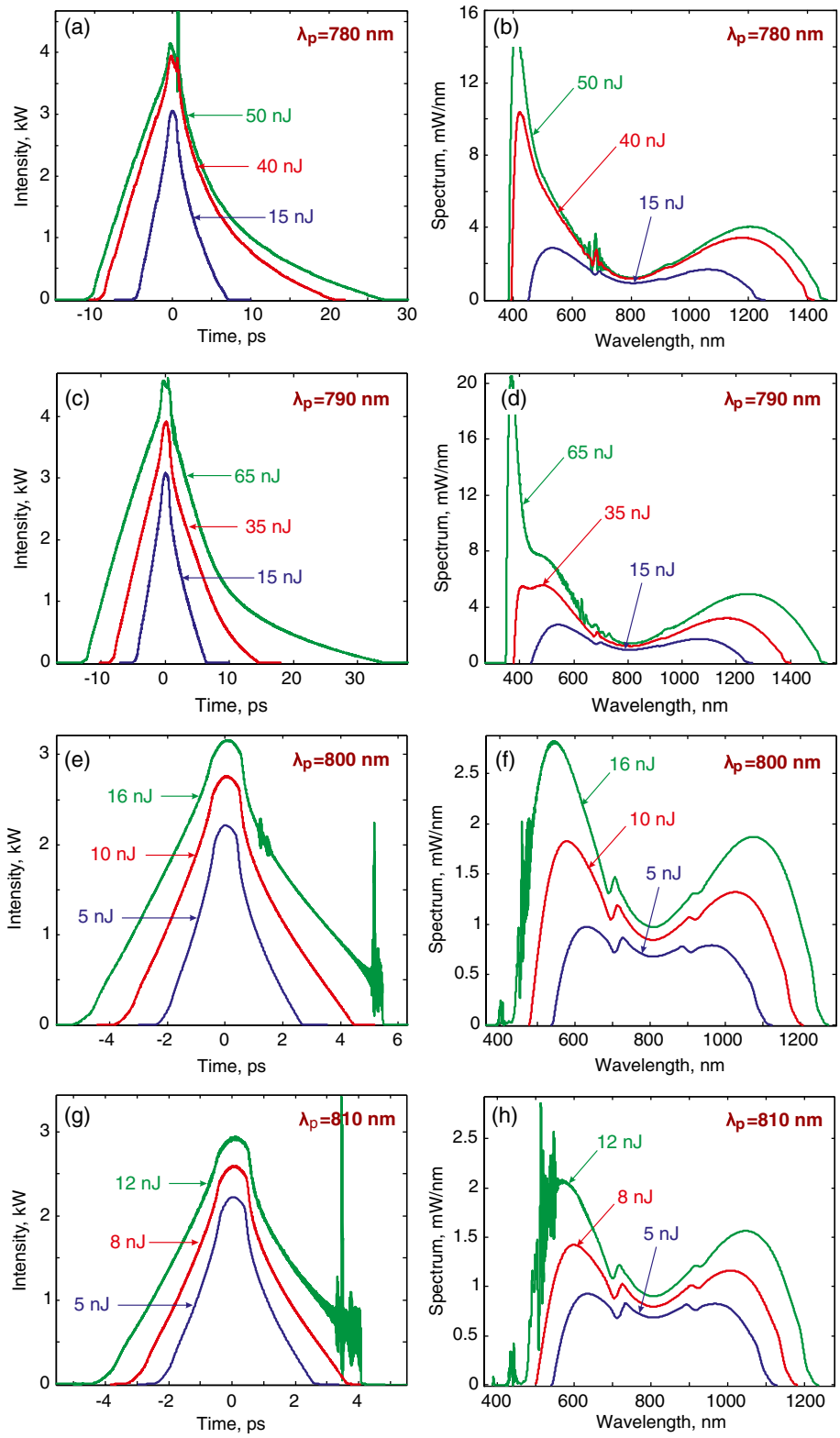


**Fig. 4** SPSC spectra (b, d, f, h) and corresponding broadened pulses (a, c, e, g) at the output of designed ANDi-MOF for different pump wavelengths and initial pulse energies. Fiber length is 10 cm.

wavelengths. However, we observe exactly the opposite situation: the appearance of the optical shock depends notably on the wavelength. Previously, in an analysis of narrow-band pulses,[14] we demonstrated that the third-order dispersion could be the cause of shock-like oscillations in both the spectral and time domains: with increasing third-order dispersion in a fiber, stronger oscillations are observed. The ANDi-MOF presented here demonstrates a variation of the third-order dispersion of more than 3.5 times within the range of pulse wavelengths considered: $\beta_3(790\ \text{nm}) = -3.9 \times 10^{-3}\ \text{ps}^3/\text{km}$, $\beta_3(800\ \text{nm}) = -8.65 \times 10^{-3}\ \text{ps}^3/\text{km}$, and $\beta_3(810\ \text{nm}) = -13.8 \times 10^{-3}\ \text{ps}^3/\text{km}$. This observation agrees fully with the results of Ref. 14. Thus, we can conclude that the shock-like signatures in Fig. 3 are due to the third-order dispersion of the designed ANDi-MOF.

## 5 Conclusion

An ANDI-MOF possessing a maximum of the dispersion curve $D(\lambda)$ at 800 nm and normal dispersion spanning more than one octave around the maximum was synthesized and characterized numerically by simulating passive nonlinear pulse reshaping at a femtosecond time scale and single-pulse flat-top octave-spanning supercontinuum. The octave-spanning SPSC is readily achievable by applying 10 cm of this fiber and 100-fs pulses of a few nanojoules around 800 nm. The Gaussian picojoule pulses of femtosecond duration can be easily transformed to parabolic pulses using a 4- to 60-cm length of the designed ANDi-MOF, depending on the preference of the experimentalists. Thus, the fiber provides a low-cost solution to develop SC sources on the basis of the femtosecond oscillators available in laboratories. Another benefit provided by the fiber is a simple, low-cost solution to the problems of arbitrary wave-form generation for the needs of, for example, optical signal processing.

## Acknowledgments

This work was partially supported by SEP/PROMEP (project UGTO-PTC-371) and the University of Guanajuato (projects DAIP-334/13 and DAIP-192/13). Oleksiy V. Shulika developed the fiber design and models used in the article; he contributed to the implementation of the calculations and data analysis and the generation of ideas on ANDi-MOF applications. Igor A. Sukhoivanov is the corresponding author and contributed to formulating the problem, justifying the initial parameters, and providing data for calculation; he also contributed to the development of the conclusions. Gabriel Ramos-Ortiz contributed by analyzing the practical applications of the obtained results. Igor V. Guryev was involved in the implementation of the numerical models and methods. Sergii O. Iakushev provided an overview and analysis of the approaches to the creation of parabolic femtosecond pulses and supercontinua; he contributed with coding and simulations. José Amparo Andrade Lucio contributed through data processing and analysis.

## References

1. J. M. Dudley, G. Genty, and S. Coen, "Supercontinuum generation in photonic crystal fiber," *Rev. Mod. Phys.* **78**(4), 1135–1184 (2006), http://dx.doi.org/10.1103/RevModPhys.78.1135.
2. A. M. Heidt et al., "Coherent octave spanning near-infrared and visible supercontinuum generation in all-normal dispersion photonic crystal fibers," *Opt. Express* **19**(4), 3775–3787 (2011), http://dx.doi.org/10.1364/OE.19.003775.
3. A. M. Heidt et al., "High quality sub-two cycle pulses from compression of supercontinuum generated in all-normal dispersion photonic crystal fiber," *Opt. Express* **19**(15), 13873–13879 (2011), http://dx.doi.org/10.1364/OE.19.013873.
4. A. Hartung, A. M. Heidt, and H. Bartelt, "Design of all-normal dispersion microstructured optical fibers for pulse-preserving supercontinuum generation," *Opt. Express* **19**(8), 7742–7749 (2011), http://dx.doi.org/10.1364/OE.19.007742.

5. S. Boscolo and C. Finot, "Nonlinear pulse shaping in fibres for pulse generation and optical processing," *Int. J. Opt.* **2012**, 159057 (2012), http://dx.doi.org/10.1155/2012/159057.
6. J. M. Dudley et al., "Self-similarity in ultrafast nonlinear optics," *Nat. Phys.* **3**(9), 597–603 (2007), http://dx.doi.org/10.1038/nphys705.
7. C. Finot et al., "Optical parabolic pulse generation and applications," *IEEE J. Quantum Electron.* **45**(11), 1482–1489 (2009), http://dx.doi.org/10.1109/JQE.2009.2027446.
8. C. Finot, S. Pitois, and G. Millot, "Regenerative 40 Gbit/s wavelength converter based on similariton generation," *Opt. Lett.* **30**(14), 1776–1778 (2005), http://dx.doi.org/10.1364/OL.30.001776.
9. F. Parmigiani et al., "Pulse retiming based on XPM using parabolic pulses formed in a fiber Bragg grating," *IEEE Photonics Technol. Lett.* **18**(7), 829–831 (2006), http://dx.doi.org/10.1109/LPT.2006.871848.
10. S. Boscolo, S. K. Turitsyn, and K. J. Blow, "Time domain all-optical signal processing at a RZ optical receiver," *Opt. Express* **13**(16), 6217–6227 (2005), http://dx.doi.org/10.1364/OPEX.13.006217.
11. T. T. Ng et al., "Compensation of linear distortions by using XPM with parabolic pulses as a time lens," *IEEE Photonics Technol. Lett.* **20**(13), 1097–1099 (2008), http://dx.doi.org/10.1109/LPT.2008.924304.
12. K. Saitoh and M. Koshiba, "Empirical relations for simple design of photonic crystal fibers," *Opt. Express* **13**(1), 267–274 (2005), http://dx.doi.org/10.1364/OPEX.13.000267.
13. K. J. Blow and D. Wood, "Theoretical description of transient stimulated scattering in optical fibers," *IEEE J. Quantum Electron.* **25**(12), 2665–2673 (1989), http://dx.doi.org/10.1109/3.40655.
14. S. O. Iakushev, O. V. Shulika, and I.A. Sukhoivanov, "Passive nonlinear reshaping towards parabolic pulses in the steady-state regime in optical fibers," *Opt. Commun.* **285**(21–22), 4493–4499 (2012), http://dx.doi.org/10.1016/j.optcom.2012.06.024.
15. S. O. Iakushev et al., "Nonlinear pulse reshaping in optical fibers," in *Laser Systems for Applications*, K. Jakubczak, Ed., pp. 185–206, In-Tech, Rijeka, Croatia (2011), http://dx.doi.org/10.5772/24456.
16. I. A. Sukhoivanov et al. "Formation of parabolic optical pulses in passive optical fibers," *Proc. SPIE* **8011**, 801131 (2011), http://dx.doi.org/10.1117/12.901822.
17. S. O. Iakushev et al., "Nonlinear pulse reshaping in passive optical fibers towards quasi-parabolic waveforms," *Proc. SPIE* **8255**, 825526 (2012), http://dx.doi.org/10.1117/12.909397.
18. A. Bartels, D. Heinecke, and S. A. Diddams, "Passively mode-locked 10 GHz femtosecond Ti:sapphire laser," *Opt. Lett.* **33**(16), 1905–1907 (2008), http://dx.doi.org/10.1364/OL.33.001905.
19. H. Byun et al., "Compact, stable 1 GHz femtosecond Er-doped fiber lasers," *Appl. Opt.* **49**(29), 5577–5582 (2010), http://dx.doi.org/10.1364/AO.49.005577.
20. S. O. Iakushev, O. V. Shulika, and I. A. Sukhoivanov, "Sub-10-fs pulses produced from compression of supercontinuum generated in all-normal dispersion photonic crystal fiber," in *Frontiers in Optics Conf. /Laser Science*, Technical Digest (CD), paper FW3A.41, Optical Society of America (2012), http://dx.doi.org/10.1364/FIO.2012.FW3A.41.
21. G. P. Agrawal, *Nonlinear Fiber Optics*, 3rd ed., Academic Press, San Diego (2001).


**Oleksiy V. Shulika** received his PhD degree in optics and laser physics from V. N. Karazin National University, Ukraine, in 2008. His research interests are ultrafast optics, nonlinear optics, semiconductor optics, and device simulation. He is a member of the IEEE Photonics Society, OSA, and SPIE.

**Igor A. Sukhoivanov** received his PhD degree in 1985 and the Dr Sc degree in 2002 from V. N. Karazin National University, Kharkiv, Ukraine. His research interests include photonic devices; photonic crystal elements including the design of photonic crystal fibers; and the generation, propagation, and reshaping of ultrashort pulses in fibers. He is a senior member of the IEEE Photonics Society and OSA and a member of SPIE.

**Gabriel Ramos-Ortiz** received his PhD degree from Arizona University, Flagstaff, Arizona, in 2003. His research interests include nonlinear optics, spectroscopy and optical characterization of materials, photonics, and optoelectronics.

**Igor V. Guryev** received his PhD degree in optics and laser physics from V. N. Karazin Kharkiv National University, in 2009. His research interests include nonlinear optics, photonic crystals, and computational physics.

**Sergii O. Iakushev** received his PhD degree in optics and laser physics from V. N. Karazin Kharkiv National University. His research interests are ultrafast optics, nonlinear optics, and fiber optics. He has been a member of the IEEE Photonics Society, OSA, and SPIE.

**José Amparo Andrade Lucio** received his PhD degree from Instituto Nacional de Astrofísica, Óptica y Electrónica, Mexico, in 1999. His research interests include nonlinear optics, ultrafast optics, optical characterization of materials, optics, and photonics.